Physics Faculty Research & Creative Works

Physics

01 Jul 2017

Determination of the Energy Band Gap of Bi₂Se₃

G. Martinez

B. A. Piot

M. Hakl

M. Potemski

et. al. For a complete list of authors, see https://scholarsmine.mst.edu/phys_facwork/1706

SCIENTIFIC REP**O**RTS

OPEN

Determination of the energy band gap of Bi$_2$Se$_3$

G. Martinez[1], B. A. Piot[1], M. Hakl[1], M. Potemski[1], Y. S. Hor[2], A. Materna[3], S. G. Strzelecka[3], A. Hruban[3,4], O. Caha[5], J. Novák[5], A. Dubroka[5], Č. Drašar[6] & M. Orlita[1,7]

Despite intensive investigations of Bi$_2$Se$_3$ in past few years, the size and nature of the bulk energy band gap of this well-known 3D topological insulator still remain unclear. Here we report on a combined magneto-transport, photoluminescence and infrared transmission study of Bi$_2$Se$_3$, which unambiguously shows that the energy band gap of this material is direct and reaches $E_g = (220 \pm 5)$ meV at low temperatures.

The existence of the energy band gap, separating the conduction and valence bands, is a key characteristic of all topological insulators, which allows these materials to behave as insulators in interior, but still, to conduct electric current via specific, topologically protected states on their surfaces[1, 2].

In bismuth selenide (Bi$_2$Se$_3$) – perhaps the most representative example of 3D topological insulators – the band gap is located at the Brillouin zone center, however, the consensus regarding further details, notably its size and nature, has not yet been established. Rather large values for the band gap (above 300 meV) have been deduced using surface-sensitive techniques, ARPES and STM/STS[3–5], which also often (but not always)[6, 7] imply its indirect nature related to the pronounced "camelback" profile of the valence band. In contrast, optical experiments[8–11] consistently show a direct band gap around 200 meV. Importantly, the missing consensus about the band gap is not a minor drawback in our understanding properties of Bi$_2$Se$_3$. It is the size and nature of the band gap which are the parameters needed for interpretation of ARPES data[3, 4], most notably, for the correct positioning of the surface cone with respect to the bulk bands. For a wider band gap, the Dirac point of the surface states approaches the midgap position. A narrower band gap shifts the charge neutrality point towards the valence band, which may, for instance, explain the pronounced electron-hole asymmetry of the surface cone observed in STM/STS experiments[12].

In this paper, we address the existing controversy about the band gap of Bi$_2$Se$_3$ using an experimental approach which combines optical methods – infrared transmission and photoluminescence – with magneto-transport, successfully used in the past also for other materials, see, e.g., refs 13 and 14. We unambiguously show that the energy band gap of Bi$_2$Se$_3$ is direct and reaches $E_g = (220 \pm 5)$ meV.

Experimental Details

To determine the band gap of Bi$_2$Se$_3$, bulk crystal of this compound was grown using the modified Bridgman method where stoichiometric mixture of high purity Bi and Se elements were vacuum sealed in a quartz tube, heated up to the melting point and cooled down to room temperature with the rate of 0.1 °C/min under the temperature gradient of about 10 °C/cm along the tube length in a box furnace. As-grown crystals showed a strong n-type doping (close to 10^{19} cm^{-3}) due to selenium vacancies, which was reduced by the after-growth annealing in selenium vapors down to 10^{18} cm^{-3}, nevertheless with a certain variation of the electron density across the crystal.

The bulk crystal was characterized using x-ray diffractometer equipped with Cu x-ray tube, channel-cut germanium monochromator and scintillation detector. The standard $\theta - 2\theta$ scan is shown in Fig. 1. The observed x-ray diffraction peaks correspond well to the c-lattice parameter of $c = (28.64 \pm 0.01)$ Å in an perfect agreement with tabulated value 28.636 Å[15]. The crystal has been then sliced using microtome machine perpendicular to the c-axis of Bi$_2$Se$_3$. Two free-standing layers with the thicknesses of $d = 6.5$ and 10 μm have been chosen for this

[1]Laboratoire National des Champs Magnétiques Intenses, CNRS-UGA-UPS-INSA-EMFL, 25, avenue des Martyrs, 38042, Grenoble, France. [2]Department of Physics, Missouri University of Science and Technology, Rolla, MO 65409, USA. [3]Institute of Electronic Materials Technology, ul. Wolczynska 133, 01-919, Warsaw, Poland. [4]Institute of Physics, Polish Academy of Science, Warsaw, PL-02668, Poland. [5]CEITEC MU, Masaryk University, Faculty of Science, 61137, Brno, Czech Republic. [6]Institute of Applied Physics and Mathematics, Faculty of Chemical Technology, University of Pardubice, Studentská 84, CZ-532 10, Pardubice, Czech Republic. [7]Institute of Physics, Charles University in Prague, CZ-121 16, Prague, Czech Republic. Correspondence and requests for materials should be addressed to M.O. (email: milan.orlita@lncmi.cnrs.fr)
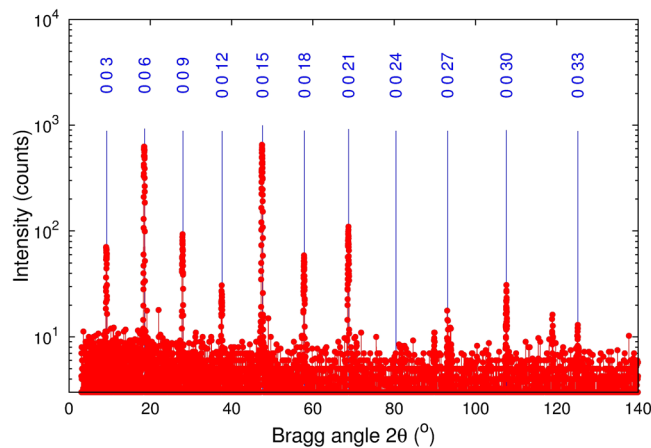
Figure 1. XRD symmetric scan collected from a Bi_2Se_3 sample. Blue lines denote theoretical positions of the diffraction peaks according to the structural database[15].

study denoted as samples A and B, respectively. They were explored in low temperature photoluminescence (PL), infrared transmission and magneto-transport experiments.

To measure PL spectra, the samples were placed in a helium bath cryostat and excited by $\lambda = 660\,nm$ diode laser with an approximate power of $100\,\mu W$ focused on spot of $1\,mm^2$. The collected signal was delivered to a Fourier transform spectrometer, analyzed and detected by a liquid-nitrogen-cooled MCT detector. To measure infrared transmission, a macroscopic area of the sample ($\approx 3\,mm^2$) was exposed to the radiation of a globar, which was analyzed by a Fourier transform spectrometer, using light-pipe optics delivered to the sample placed in a helium bath cryostat and detected by a composite bolometer placed just below the sample. Magneto-transport experiments were conducted on samples contacted using silver paste in the Van der Pauw-like geometry. Measurements were performed using a standard low-frequency lock-in technique in a variable temperature insert, with the magnetic field applied along the c-axis of Bi_2Se_3.

Discussion

We start the discussion with the PL spectra recorded from both samples at liquid-helium temperatures (Fig. 2a and b). It is just the existence of a well-defined efficient PL emission, which clearly indicates a direct nature of the band gap in Bi_2Se_3. In other words, the conduction-band electrons are located around the same point of the Brillouin zone as the photo-excited holes in the valence band. The positions of the observed PL emission in spectra then provide us with the very first estimate for the size of the band gap.

In the simplest possible scenario, one may assume that the the observed PL corresponds to a direct band-to-band (vertical in k-space) recombination of electrons from the degenerate gas at the bottom of the conduction band with photo-excited holes at the top of the valence band. In such a case, the band gap can be associated with the inflection point at the low-energy onset of PL emission line, having for both samples the energy close to 220 meV and denoted in Fig. 2a and b by vertical dashed lines. From other, more complex scenarios for PL mechanisms, we may exclude, due to screening effects in the degenerate electron gas, the excitonic-like recombination. However, one may still imagine a variety of defects-related radiative recombination channels, often efficient in semiconducting compounds and giving rise to sub-band-gap emission of light. The photon energy of the PL emission thus serves only as a lower bound for the (direct) band gap in Bi_2Se_3.

Another estimate of the band gap E_g, in this case implying its upper bound, comes from the analysis of the infrared transmission (Fig. 2c and d). Both samples show rather broad transparency window, which is at low photon energies limited by the free carrier response (reflectivity below the plasma edge) and also by the absorption due to infrared active phonons[16]. At high photon energies, the transmission window closes due to a relatively sharp onset of interband absorption. This onset is often referred to as the optical band gap E_g^{opt} and represents the upper bound for the band gap due to the well-known Moss-Burstein shift that is characteristic of semiconductors with a degenerate electron or hole gas (see the inset of Fig. 2a)[17].

The approximate position of the optical band gap is denoted in Fig. 2c and d by the vertical arrow. A more precise read-out of E_g^{opt} is possible when transmission is plotted as absorbance and normalized by the sample thickness (insets of Fig. 2c,d). When the optical band gap is approached, the absorbance becomes dominantly governed by absorption: $\alpha \approx -\ln(T)/d$, which increases almost exponentially that is reminiscent of the Urbach edge absorption in (undoped) semiconductors[18]. The optical band gap may then be associated with the photon energy at which the absorption coefficient α approaches $10^4\,cm^{-1}$, a value typical for interband absorption in direct-band-gap semiconductors[19]. For the sample A and B, we obtain $E_g^{opt,A} = (250 \pm 3)$ meV and $E_g^{opt,B} = (258 \pm 3)$ meV, respectively.

To extract the size of the band gap E_g from E_g^{opt}, the Moss-Burstein shift has to be estimated. In a degenerate n-type semiconductor with a direct band gap, this shift reads: $\Delta E_{MB} = E_g^{opt} - E_g = (1 + m_e/m_h)E_F$, where E_F is the Fermi energy and $m_{e(h)}$ stands for the electron (hole) effective mass. The anisotropy of effective masses enters this expression only, when the ratio m_e/m_h becomes strongly anisotropic, which does not seem to be the case of
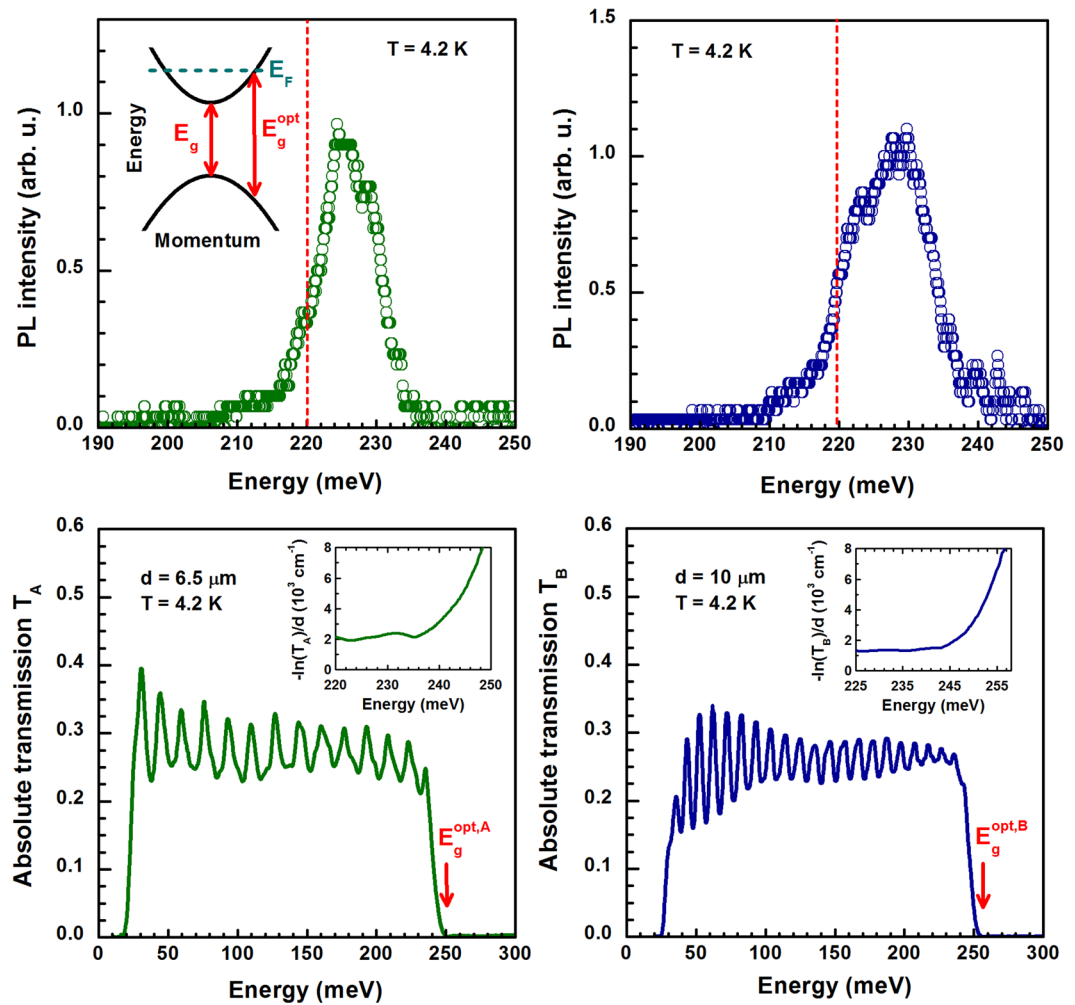
Figure 2. (**a,b**) Low-temperature PL spectra collected from samples A and B, respectively. The dashed vertical lines denote the estimated energy of the band gap, see the discussion in the main text. The schematic band structure of Bi_2Se_3 is plotted in the inset of the part (**a**), the difference between E_g and E_g^{opt} corresponds to the Moss-Burstein shift. (**c,d**): Infrared transmission data T_A and T_B taken on samples A and B, respectively. The corresponding absorbance spectra, $-\ln(T)/d$, around the interband absorption edge E_g^{opt}, normalized by the sample thickness, are plotted in the insets. The pronounced modulation of the transmission spectra is due to Fabry-Pérot oscillations, which show rather high crystalline quality of the studied Bi_2Se_3 bulk samples and which allows us to estimate, knowing the thickness of the samples, the refraction index: $n \approx 5.5\text{–}6$.

Bi_2Se_3[20, 21]. This formula is valid only for systems with well-defined effective masses, and therefore strictly parabolic bands. Nevertheless, it is the existence of the direct band gap (implied by our PL data), which ensures such a parabolicity of bands, at least in the vicinity of the band edges. Let us also note, the parabolic shape of both, conduction and valence, bands is also consistent with results of magneto-transport experiments performed on bulk Bi_2Se_3 specimens[20–23] and Landau level spectroscopy on thin epitaxial layers[11].

Importantly, the Moss-Burstein shift may be expressed as $\Delta E_{MB} = e\hbar F/\mu$, where μ stands for the reduced mass, $m_e m_h/(m_e + m_h)$, and F is the characteristic frequency of the $1/B$-periodic quantum oscillations, $F = m_e E_F/(\hbar e)$, which are associated with the Landau quantization of electrons, emerging under an externally applied magnetic field. These were clearly resolved in the magneto-transport data in a form of Shubnikov-de Haas effect (Fig. 3a and b). In both samples, a single oscillation frequency has been found, $F_A = 22.0 \pm 0.5$ T and $F_B = 28.0 \pm 0.5$ T, consistently with expectations for a degenerate electron gas in a simple parabolic conduction band. Let us note that the observed Shubnikov-de Haas oscillations originate in bulk states of Bi_2Se_3. The contribution of the surface states to the transport response remains at given bulk electron densities negligible.

This may clearly demonstrated, *e.g.*, by the angle dependence of Shubnikov-de Haas oscillations, which we have studied on samples coming from the same batch in the scope of our preceding NMR study, see ref. 23 and the related Supplementary Materials. These magneto-transport experiments also implied (via damping of Shubnikov-de Haas oscillations with temperature) the effective mass of bulk conduction band electrons, $m_e \approx 0.12m_0$, which agrees well with values from previous studies[20, 22, 24–26]. Combining this electron mass with the hole mass from our recent magneto-transport studies performed on p-type Bi_2Se_3[21], $m_h \approx 0.24m_0$, we obtain
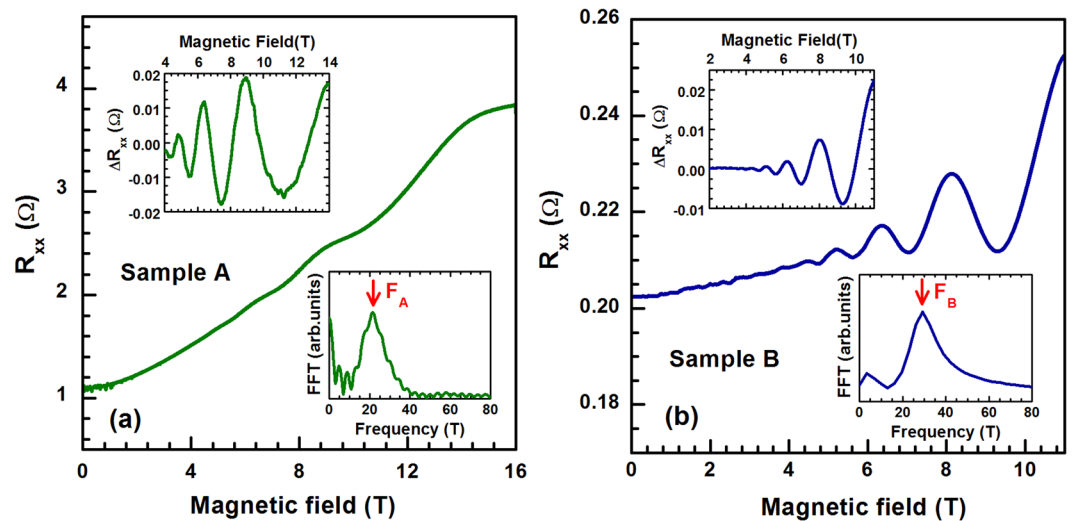
Figure 3. (**a,b**) Magneto-resistance data on samples A and B taken at the temperature of $T = 4.2$ and $1.4\,\mathrm{K}$, respectively. The upper and lower insets show background-removed data ΔR_{xx} and fast Fourier transform of $\Delta R_{xx}(B^{-1})$, respectively. The latter imply the oscillation frequencies $F_A = 22.0 \pm 0.5\,\mathrm{T}$ and $F_B = 28.0 \pm 0.5\,\mathrm{T}$ for the samples A and B, respectively.

the reduced mass of $\mu \approx 0.08 m_0$, in perfect agreement with the value read directly from the separation of inter-band inter-Landau level resonances observed in our recent magneto-optical study[11].

Taking account of the Shubnikov-de Haas oscillation frequencies and the estimated effective reduce mass, we get the Moss-Burstein shifts of $\Delta E_{MB}^A \approx 30\,\mathrm{meV}$ and $\Delta E_{MB}^B \approx 40\,\mathrm{meV}$ for the sample A and B, respectively. Subtracting these values from the optical band gaps $E_g^{\mathrm{opt,A}}$ and $E_g^{\mathrm{opt,B}}$, we obtain at the energy band gap of Bi_2Se_3: $E_g = (220 \pm 5)\,\mathrm{meV}$. This value is in perfect agreement with the PL results, when the simplest scenario of direct band-to-band recombination of free electrons and holes is considered. Let us also note that we do not consider the band gap renormalization, which for electron densities close to $10^{18}\,\mathrm{cm}^{-3}$ provides us with a correction of the band gap well below the estimated error bar[27].

Let us emphasize that the extracted band gap, $E_g = (220 \pm 5)\,\mathrm{meV}$, as well as its direct nature clearly contrasts with conclusions of several ARPES experiments performed on bulk Bi_2Se_3[3–5], nevertheless not with all of them, see, *e.g.*, refs 6 and 7 This technique thus seems to be well-suited for investigations of surface properties and the observation of conical bands on the surface of topological insulators is definitely one of its greatest achievements[28]. At the same time, the visualization of a truly bulk electronic band structure, especially in narrow gap materials, which are characterized by pronounced band bending effects[29] and charge accumulation layers on the surface, may be a challenging task for the surface-sensitive techniques, with a strongly limited penetration depth.

Conclusions

In summary, we have explored bulk Bi_2Se_3 using magneto-transport and infrared spectroscopy techniques aiming at determining the nature and size of the energy band gap in this 3D topological insulator. We have shown that the energy band gap is direct and falls into the interval of $E_g = (220 \pm 5)\,\mathrm{meV}$.

References

1. Hasan, M. Z. & Kane, C. L. Colloquium: Topological insulators. *Rev. Mod. Phys.* **82**, 3045–3067 (2010).
2. Qi, X.-L. & Zhang, S.-C. Topological insulators and superconductors. *Rev. Mod. Phys.* **83**, 1057–1110 (2011).
3. Xia, Y. *et al*. Observation of a large-gap topological-insulator class with a single dirac cone on the surface. *Nature Phys* **5**, 398–402 (2009).
4. Bianchi, M. *et al*. Coexistence of the topological state and a two-dimensional electron gas on the surface of bi2se3. *Nature Comm.* **1** (2010).
5. Kim, S. *et al*. Surface scattering via bulk continuum states in the 3d topological insulator bi2se3. *Phys. Rev. Lett.* **107**, 056803 (2011).
6. Chen, Y. L. *et al*. Massive dirac fermion on the surface of a magnetically doped topological insulator. **329**, 659–662 (2010).
7. Nechaev, I. A. *et al*. Evidence for a direct band gap in the topological insulator bi2se3 from theory and experiment. *Phys. Rev. B* **87**, 121111 (2013).
8. Gobrecht, H., Seeck, S. & Klose, T. Der einfluß der freien ladungsträger auf die optischen konstanten des bi2se3 im wellenlängengebiet von 2 bis 23 μm. *Zeitschrift für Physik* **190**, 427–443 (1966).
9. Köhler, H. & Hartmann, J. Burstein shift of the absorption edge of n-bi2se3. *phys. stat. sol. (b)* **63**, 171–176 (1974).
10. Post, K. W. *et al*. Thickness-dependent bulk electronic properties in bi2se3 thin films revealed by infrared spectroscopy. *Phys. Rev. B* **88**, 075121 (2013).
11. Orlita, M. *et al*. Magneto-optics of massive dirac fermions in bulk bi2se3. *Phys. Rev. Lett.* **114**, 186401 (2015).
12. Cheng, P. *et al*. Landau quantization of topological surface states in bi2se3. *Phys. Rev. Lett.* **105**, 076801 (2010).
13. Wu, J. *et al*. Unusual properties of the fundamental band gap of inn. *Applied Physics Letters* **80**, 3967–3969 (2002).
14. Wu, J. *et al*. Small band gap bowing in in 1−xgaxn alloys. *Applied Physics Letters* **80**, 4741–4743 (2002).
15. The crystal structure of bi2te3−xsex. *Journal of Physics and Chemistry of Solids* **24**, 479–485 (1963).
16. Richter, W., Kohler, H. & Becker, C. Raman and far-infrared investigations of phonons in rhombohedral V2–VI3 compounds - Bi2Te3, Bi2Se3, Sb2Te3 and Bi2(Te1−xSex)3 (0 < x < 1), (Bi1−ySby)2Te3 (0 < y < 1). *physica status solidi b* **84**, 619–628 (1977).

17. Burstein, E. Anomalous optical absorption limit in insb. *Phys. Rev* **93**, 632–633 (1954).
18. Urbach, F. The long-wavelength edge of photographic sensitivity and of the electronic absorption of solids. *Phys. Rev* **92**, 1324–1324 (1953).
19. Yu, P. Y. & Cardona, M. *Fundamentals of Semiconductors* (Springer, Berlin Heidelberg, 2010).
20. Köhler, H. Conduction band parameters of bi_2se_3 from shubnikov-de haas investigations. *Phys. stat. sol.* (*b*) **58**, 91–100, http://onlinelibrary.wiley.com/doi/10.1002/pssb.2220580109/abstract (1973).
21. Piot, B. A. *et al*. Hole fermi surface in bi_2se_3 probed by quantum oscillations. *Phys. Rev. B* **93**, 155206 (2016).
22. Fauqué, B. *et al*. Magnetothermoelectric properties of bi_2se_3. *Phys. Rev. B* **87**, 035133 (2013).
23. Mukhopadhyay, S. *et al*. Hyperfine coupling and spin polarization in the bulk of the topological insulator bi_2se_3. *Phys. Rev. B* **91**, 081105 (2015).
24. Sushkov, A. B. *et al*. Far-infrared cyclotron resonance and faraday effect in bi_2se_3. *Phys. Rev. B* **82**, 125110 (2010).
25. Butch, N. P. *et al*. Strong surface scattering in ultrahigh-mobility bi_2se_3 topological insulator crystals. *Phys. Rev. B* **81**, 241301 (2010).
26. Eto, K., Ren, Z., Taskin, A. A., Segawa, K. & Ando, Y. Angular-dependent oscillations of the magnetoresistance in bi_2se_3 due to the three-dimensional bulk fermi surface. *Phys. Rev. B* **81**, 195309 (2010).
27. Auvergne, D., Camassel, J. & Mathieu, H. Band-gap shrinkage of semiconductors. *Phys. Rev. B* **11**, 2251–2259 (1975).
28. Hsieh, D. *et al*. A topological dirac insulator in a quantum spin hall phase. *Nature* **452**, 970–974 (2008).
29. Veyrat, L. *et al*. Band bending inversion in bi_2se_3 nanostructures. *Nano Letters* **15**, 7503–7507 (2015).

Acknowledgements

Author Contributions

G.M., M.O. and M.P. conceived the study. Experiments were performed by B.A.P., M.H., G.M., and M.O. The samples were prepared and characterized by Y.S.H., A.M., S.G.S., C.D., A.H., O.C. and J.N. The data were analyzed by G.M., M.P., B.A.P., A.D., O.C., J.N. and M.O. The manuscript was written by M.O. and G.M. All authors discussed the results and commented on the manuscript.

Additional Information